Published in final edited form as:
J Phys Chem B. 2010 June 10; 114(22): 7692–7702. doi:10.1021/jp103098r.

Multireference *Ab Initio* Calculations of g tensors for Trinuclear Copper Clusters in Multicopper Oxidases

Steven Vancoillie[‡], **Jakub Chalupský**[§], **Ulf Ryde**[‖], **Edward I. Solomon**[⊥], **Kristine Pierloot**[‡], **Frank Neese**[¶,*], and **Lubomír Rulíšek**[§,*]

[‡]Department of Chemistry, University of Leuven, Celestijnenlaan 200F, B-3001 Heverlee-Leuven, Belgium

[§]Institute of Organic Chemistry and Biochemistry of the Academy of Sciences of the Czech Republic, Gilead Sciences Research Center & IOCB, Flemingovo náměstí. 2, 166 10 Praha 6, Czech Republic

[‖]Department of Theoretical Chemistry, Lund University, Chemical Center, P.O. Box 124, S–221 00 Lund, Sweden

[⊥]Department of Chemistry, Stanford University, Stanford, California 94305, U. S. A

[¶]Institut für Pysikalische und Theoretische Chemie, Universität Bonn, Wegelerstrasse 12, D-53115 Bonn, Germany

Abstract

EPR spectroscopy has proven to be an indispensable tool in elucidating the structure of metal sites in proteins. In recent years, experimental EPR data have been complemented by theoretical calculations, which have become a standard tool of many quantum chemical packages. However, there have only been a few attempts to calculate EPR **g** tensors for exchange-coupled systems with more than two spins. In this work, we present a quantum chemical study of structural, electronic, and magnetic properties of intermediates in the reaction cycle of multicopper oxidases and of their inorganic models. All these systems contain three copper(II) ions bridged by hydroxide or O^{2-} anions and their ground states are antiferromagnetically coupled doublets. We demonstrate that only multireference methods, such as CASSCF/CASPT2 or MRCI can yield qualitatively correct results (compared to the experimental values) and consider the accuracy of the calculated EPR **g** tensors as the current benchmark of quantum chemical methods. By decomposing the calculated **g** tensors into terms arising from interactions of the ground state with the various excited states, the origin of the zero-field splitting is explained. The results of the study demonstrate that a truly quantitative prediction of the **g** tensors of exchange-coupled systems is a great challenge to contemporary theory. The predictions strongly depend on small energy differences that are difficult to predict with sufficient accuracy by any quantum chemical method that is applicable to systems of the size of our target systems.

1. Introduction

Electron paramagnetic resonance (EPR) spectroscopy is an indispensable technique in elucidating the structural and electronic properties of metal-containing active sites in proteins. [1] As such, it has been challenging for theoretical chemists to calculate, interpret, or predict the

[*] Corresponding authors. Tel.: +420-220-183-263, Fax: +420-220-183-578 (LR), rulisek@uochb.cas.cz; neese@thch.uni-bonn.de.

SUPPORTING INFORMATION PARAGRAPH. The atomic coordinates of the studied systems, the broken symmetry DFT calculations (theory and applications), Tables S1–S4 and Figures S1–S11. This material is available free of charge via the Internet at http://pubs.acs.org.

experimental EPR spectra, in particular **g** tensors.[2,3,4] Since the methodological development is well documented in recent articles and reviews,[5,6,7,8,9,10,11] we only mention that the calculation of **g** tensor for organic radicals or transition-metal containing systems with a single unpaired electron is becoming a standard tool in the arsenal of quantum chemistry.[12,13,14,15,16] However, there are still systems that are difficult to treat with a satisfactory accuracy.[17] Notably, copper(II) containing systems have been a challenge to quantum chemical methods.[18,19,20,21,22,23] The situation is even worse for exchange-coupled systems containing various patterns of coupling of several unpaired electrons.[24]

Recently, we made an attempt[25] to investigate the structural, magnetic, and electronic properties of heterospin polymer chain complexes of Cu^{2+} hexafluoroacetylacetonate containing –$NO^{\bullet}$-Cu(II)-$NO^{\bullet}$-spin triads.[26] These systems exhibit peculiar magnetic properties, such as structural transitions at low temperatures.[27,28] It was convincingly shown that multireference *ab initio* calculations (complete active space self consistent field, CASSCF combined with complete active space second-order perturbation theory, CASPT2) can explain these experimental observations and that calculated *g* factors ($g_{||} = 1.848$, $g\perp = 1.974$) qualitatively reproduce the observed $g < 2$ signals in the experimental low-temperature EPR spectra.

It is therefore tempting to tackle biologically relevant systems and related inorganic model complexes with more complex electronic structures using the same computational methodology. In this work, we study coupled trinuclear copper clusters (TNC), bridged by hydroxy or oxo ligands.[29] The TNC is a unique feature of multicopper oxidases (MCO), i.e. enzymes that couple four one-electron oxidations of a substrate with the four-electron reduction of molecular oxygen to water.30

A plethora of spectroscopic data can be found in the literature for many enzymes in the MCO family, in particular for the most studied member of the family, laccase (Lc).[31,32] These experimental studies33,34,35 together with the available structural information36,[37] have yielded essential mechanistic information regarding the MCO reaction mechanism. They have been further supported by combined quantum mechanics/molecular mechanics (QM/MM) calculations,[38] multireference CASPT2 calculations of excited states of model trinuclear copper clusters representing the MCO intermediates,39 and combined EXAFS/QM/MM calculations.40 Specifically, two intermediates have been observed, the so-called peroxy intermediate33 (PI Figures 1a and 1b) and native intermediate[35] (NI). Of these, the NI is EPR active and has been shown to be a four-electron reduced product of O_2, bound to a fully oxidized trinuclear cluster.[35] It has a total spin of 1/2 and shows electronic coupling over all three copper ions in the trinuclear cluster.[35] The most plausible structure is depicted on Figure 1c (denoted as NI_C). However, there are also alternative proposals. Figure 1d depicts an alternative structure for the NI that is referred to as NI_S (containing three OH^- ions, each bridging two of the Cu ions in the trinuclear cluster).[35,38]

The MCO resting state (Figure 1e) and the non-catalytic peroxy adduct (PA, Figure 1f) have also been characterized experimentally and theoretically.[38,39,41] Finally, two inorganic models of the two alternative structural interpretations of the NI have been synthesized and studied experimentally, a D_3-symmetric trinuclear tris(μ-hydroxy)tricopper(II) cluster (TrisOH) and a C_3-symmetric μ_3-oxo-bridged trinuclear Cu(II) model (μ_3O), depicted in Figures 1g and 1h, respectively.[42,43,44,45] Comparative variable-temperature variable-field MCD studies indicated that the latter structure is the better model of the native intermediate.[45]

The aim of this work is to approach the calculation of the magnetic properties of such intricate spin-coupled systems using wave-function based *ab initio* methodology. We believe that these methods are presently without alternative for tackling problems of this kind. Hence, we have

applied various multireference approaches (CASPT2, difference dedicated configuration interaction, DDCI, single-excitation based multireference configuration interaction, MRCI-S) for the calculations of **g** tensors for the above models of MCO intermediates. Once the methods are validated one can hope to use them in the structural elucidation of observed intermediates in enzymatic reactions using EPR **g** tensors.

2. Discussion of methodological challenges in multireference *ab initio* calculations on spin coupled systems

In a conventional paramagnetic molecule, N unpaired electrons are typically coupled in parallel to give a state with $S = N/2$ (which is referred to as the high-spin coupling case). Such a state is well described by a single Slater determinant, e.g. in Hartree–Fock or Kohn–Sham density functional theory. Provided that there is no low-lying excited state of the same spin (e.g. lower than the spin–orbit coupling constant which is on the order of a few hundred wavenumbers), then the spin–orbit coupling (SOC) between the ground state and the singly-excited states of the same total spin determines the angular momentum in the ground state and hence the molecular **g** tensor. While conceptually only singly-excited states are required, actual wave-function based *ab initio* computations also need to include higher excitations in order to describe the electronic relaxation in the excited states relative to the ground state even if these are dominated by single excitations. Electronic relaxation is a consequence of employing calculations based on fixed molecular orbitals that are typically optimized for the ground state. However, a complete calculation would require a summation over all excited states, which is obviously not possible. Thus, it is more convenient and more satisfying to resort to linear-response theory, which is equivalent to a complete sum over states, while being computationally more tractable.[46] Consequently, the majority of **g** tensor calculations are now based on linear-response theory. In many cases, the results are satisfactory.

There are two situations in which this standard treatment becomes inappropriate. The first situation is the case of exact or near orbital degeneracy. Then, the SOC effects become equal or larger than the excitation energies and a first-order correction to the non-relativistic ground-state wave function is not sufficient. Thus, one must treat the SOC to all orders. In order to obtain a balanced basis for such a treatment, it is necessary to determine the low-lying states on an equal footing through a multiconfigurational treatment, most conveniently offered by a CASSCF calculation (this defines the model space).[47] Since the SOC between the ground state and the low-lying states is very strong (unless forbidden by symmetry), this single component would dominate the sum over states and then it is appropriate to just rediagonalize the SOC operator in the basis of a few non-relativistic roots of the Born-Oppenheimer Hamiltonian (quasi-degenerate perturbation theory, QDPT). However, this requires the inclusion of all magnetic sublevels $M_S = S, S\text{-}1, \ldots, -S$ for each state with a total spin S. All required matrix elements can be conveniently generated from the principal components with $M_S = S$ through application of the Wigner–Eckart theorem.[48,49] The **g** tensor can then be found separately for each Kramers doublet arising from the diagonalization of the SOC operator through first-order perturbation theory with the Zeeman operator. Such calculations have been commonplace in ligand-field (LF) theory for a long time[50] and have been carried over to multiconfigurational *ab initio* quantum chemistry by several authors.[17,51,52]

The second situation in which standard linear-response theory is insufficient involves spin-coupled systems where the unpaired electrons do not line up to give the maximum total spin of $S = N/2$ but rather couple to a lower total spin. In this case, the ground state and all excited states are multideterminantal (but not necessarily multiconfigurational). The only feasible way to generate these states of given total spin correctly is multiconfigurational quantum chemistry. Again, the same QDPT protocol can then be followed for the calculation of the **g** tensor. However, in the spin-coupled case, there are additional challenges: (i) there is not necessarily

a single low-lying excited state that dominates the SOC, and (ii) due to the intricacies of spin coupling there are many more excited states to be handled than in the case of a simple high-spin ground state.

A particular situation of this kind is met in oligonuclear transition-metal systems such as those studied here. For mononuclear Cu(II) complexes, it is reasonable to assume that the sum-over-states is dominated by the four excited LF states. Thus, if their energies and the covalency of the ground state are correctly described, one should obtain reasonable **g** tensor predictions. Several studies along these lines have been published, based on CASSCF/CASPT2[17,18] or multireference configuration interaction (MRCI) calculations.[51] In the case of the copper trimer, however, there are three unpaired electrons and such a situation gives rise to one quartet and two doublet states. Of these, only the quartet state is of high-spin and can thus be straightforwardly treated. The two doublet states are multideterminantal and do not directly spin-orbit couple, since SOC between states that have the same orbital configuration vanishes. However, there are now fifteen *d* orbitals to be included in the treatment and each local *d*–*d* excitation gives also rise to two doublet states. Thus, there is a total of 26 doublet states (ground plus three times four LF excited states) with *d*–*d* character that need to be explicitly represented in the calculations to develop at a realistic calculation of the **g** tensor.

Unfortunately, it is not sufficient to simply obtain a CASSCF wave function that is the average over all these LF states, because CASSCF suffers severely from the characteristic Hartree–Fock imbalance of having too ionic metal–ligand bonds.[7,18] Thus, one either needs to obtain better orbitals at the CASSCF step or to repair the deficiencies of the orbitals in the post-CASSCF calculation.

The former choice is the strategy followed in CASPT2 calculations. Given the CASSCF states, one calculates a second-order perturbation correction with a contracted expansion of the first-order correlated wave function. Due to the contraction and the low-order perturbation treatment, the correlated wave function does not relax the electronic structure. Thus, one only obtains good results, if the reference CASSCF wave function already provides a good starting point. In many transition-metal complexes this requires a second *d* shell to be included in the active space (the so-called “double-shell” effect)[53] and in addition one needs to average over the relevant ligand-to-metal charge-transfer states (LMCT) and consider a multistate CASPT2 (MS-CASPT2) treatment18 in order to obtain more realistic metal–ligand covalencies. At this point, the calculations become so demanding that they are restricted to mononuclear complexes.

The alternative choice of relaxing the orbitals in the correlation calculation is the strategy followed in uncontracted multireference configuration interaction (MRCI) treatments. Here one performs single and double excitations relative to all reference determinants. Upon diagonalization of the nonrelativistic Hamiltonian to all orders, one obtains a fully relaxed electronic structure and realistic charge and spin distributions. However, there are at least two drawbacks to this approach. First, the straightforward diagonalization leads to size-inconsistent results and hence the quality of the treatment deteriorates for larger molecules. Second, the number of single and double excitations relative to a reasonably large reference CASSCF space is excessive. Hence the computational effort to perform the calculation quickly becomes unmanageable, in particular because diagonalization is several orders of magnitude more expensive than second-order perturbation theory. The problems can, to some extent, be dealt with by contracting the excited configuration state functions (CSFs) rather than performing individual excitations relative to each reference and by including only a limited number of excitation classes in the treatment. Contraction is highly complex and there exists no program that could be applied to larger molecules. The limited excitation class treatment amounts to Malrieu’s concept of DDCI which has been successful in the calculations of exchange

couplings and related properties.[54] However, if the systems become large, the reference space becomes large, many roots are required (which is the case for all the complexes in the present study), and even the most efficient variant of DDCI becomes computationally unfeasible.

Based on these considerations, it becomes evident that there presently does not exist a single computational protocol that would allow one to perform fully satisfactory first-principle **g** tensor calculations on a spin-coupled system such as the tricopper complexes studied here. In the course of the study, we thus resorted to the following two approaches:

(i) A CASSCF/CASPT2 treatment in which all fifteen *d* orbitals are included in the active space, CASSCF(27,15). The high efficiency of the CASSCF/CASPT2 method allows one to calculate the appropriate number of doublet roots for this reference space and then use the state-interaction concept to compute the SOC between the relevant doublet and quartet roots. The drawback of this procedure is that neither the double-shell effect nor the LMCT states can be treated. Thus, one expects LF transition energies that are fairly reasonable because there is not much differential correlation energy in *d*–*d* excitations,[11] but *g* shifts that might be too large due to the exaggerated ionicity of the CASSCF reference states. The efficient implementation of the MOLCAS program[62] is best suited for these calculations.

(ii) A CASSCF(3,3) treatment followed by either DDCI-2 in order to obtain reasonable exchange splittings between the quartet and the two doublet states or CI with singly excited orbital configurations to obtain all relevant doublet and quartet roots (referred to as CAS(3,3)/MRCI-S). Because the singly-excited (but correctly spin-coupled) CSFs do not bring in much correlation energy, the problems of size consistency are not too severe. Also, the transition energies from CAS/MRCI-S are expected to be reasonable because of the small differential correlation energy in *d*–*d* excited states. On the other hand, single excitations are not enough to repair the deficiencies of the CASSCF orbitals, hence one also expects overestimated *g*-shifts. Such calculations can be performed with the ORCA program.[55] However, there is an important methodological issue. The ORCA MRCI program does not take advantage of contraction, but instead uses perturbation-theory based configuration selection to ease the computational burden. Since the energy differences that are the focus of this work are small, selection introduces artifacts and should not be used. This, unfortunately, greatly adds to the computational effort.

The quasi-degenerate perturbation theory that introduces SOC into the treatment is conceptually very similar in both programs. One has to calculate the matrix elements $<\Psi_I^{SM}|\boldsymbol{H}^{SOC}|\Psi_J^{S'M'}>$ for correlated state pairs *I* and *J* with total spins *S* and *S'* and projection *M* and *M'*, respectively. In the MOLCAS implementation, the correlated wave function is replaced by the reference CASSCF wave function[17] and the SOC operator is represented by the single-center atomic mean-field SOC (AMFI) operator.[13,56,57] In the ORCA implementation, the matrix elements are directly calculated over the correlated states.48 The SOC is also represented by the mean-field SOC operator, but it differs from AMFI by making neither the single-center nor the fixed atomic-density approximations.[58]

3. Computational Details

The molecular geometries used in this study correspond to the QM/MM equilibrium geometries of MCO systems and are described in detail in the preceding study.[39]

3.1. CASSCF/CASPT2 calculations

All CASSCF[59]/CASPT2[60,61] and **g**-matrix calculations were performed with MOLCAS 7.0.[62] ANO-S basis sets were used for all atoms with the following contractions: Cu [6s4p3d2f]; C, N, O [3s2p1d]; H [2s].[63] For each molecule the ground- and excited-state wave functions

were computed at the CASSCF level. Excitation energies were computed at the MS-CASPT2 level.64 The **g** tensor calculations were performed with the RASSI module, which treats SOC through the AMFI[13,65,66] approximation, using approach II for the **g** matrix.[17] Within this approach, a SOC calculation is performed first and the Zeeman effect is treated afterwards within the lowest Kramers doublet.

All calculations were performed without symmetry. However, in the case of TrisOH, D_3 symmetry was enforced by preventing rotations between orbitals belonging to different D_3 representations (e.g. using the SUPSym keyword in the MOLCAS program). At the CASSCF level, this leads to pairs of ^{2}E components that are perfectly degenerate. However, in MS-CASPT2 calculations the pairs are no longer degenerate due to symmetry breaking that arises from the internal contraction. To obtain the correct anisotropy of the *g* factors, it is crucial to keep the ^{2}E ground state exactly degenerate (if non-degeneracy is allowed, the weak SOC between the components of the ^{2}E ground state – about one wavenumber – is quenched and the calculated **g** tensors are no longer realistic). To obtain a correct anisotropy within the equatorial (*xy*) plane, it was also necessary to keep the excited ^{2}E states degenerate. Unfortunately, even when starting from degenerate CASSCF solutions the perturbation-modified complete active space (PM-CAS) wave functions produced by MS-CASPT2 for the two ^{2}E components still show a certain amount of symmetry breaking (8 cm^{-1}). As a result, the two equatorial *g* factors obtained with the latter method are not perfectly equal as they should be.

Taking into account all possible excitations where the electrons remain on the same copper center leads to 125 quartets (5×5×5) and 250 doublets (twice the number of quartets, as each single excitation with three unpaired electrons produces two linearly independent doublet states). Unfortunately, it is not possible to handle that many states with CASPT2. However, it is found that of these LF states, the lowest 13 quartets and 26 doublets, corresponding to all single (total) excitations are well separated from the other states and hence might well be sufficient for the present purposes.

Three sets of results are reported, obtained from: (1) CASSCF wave functions and excitation energies; (2) CASSCF wave functions and CASPT2 excitation energies; (3) PM-CAS wave functions and MS-CASPT2 excitation energies. For each set, the contributions of the excited states to the *g* values were analyzed using a partitioning of the terms that make up the G_{pq} values, that are the elements of the matrix $\mathbf{G} = \mathbf{g}\,\mathbf{g}\dagger$. Details can be found in the Supporting Information.

As all states contribute in some way to the final result, the analysis was confined to those states that contribute the most to the diagonal G_{pp} values. Note that this does not provide a contribution to g_{pp}, however, because the latter is essentially the square root of the sum over contributions that give G_{pp} (neglecting off-diagonal elements). To verify the importance of individual excited states, we have also performed calculations including only the most strongly contributing states. This procedure should yield results that are sufficiently close to the results obtained by including all excited states.

3.2. Variational Multireference Calculations

The multireference configuration interaction (MRCI) calculations, and CASSCF calculations used for generating input molecular orbitals for the subsequent MRCI, were carried out using the ORCA 2.6.35 program.[55] In these calculations, the def2-SV(P) basis set67 was used, which is of similar size and quality as the ANO-S bases used in the MOLCAS calculations. Indeed, the transition energies calculated at the state-average CASSCF level reported below differ negligibly between the two programs and basis sets (1–2 cm^{-1} with the exception of NI_C system, where it amounts to 11 cm^{-1}).

Two sets of variational multireference calculations were carried out:

1. Calculation of the exchange couplings were performed on the basis of CASSCF(3,3) reference states for one quartet and two doublet roots, followed by uncontracted DDCI-2 and DDCI-3 calculations. The selection thresholds T_{sel} and T_{pre} explained elsewhere in detail[68] were set to tight values of 10^{-8} a.u. and 10^{-5} a.u. in order to ensure converged state-energy differences. This convergence was checked by performing additional calculations with $T_{pre}= 0$ and $T_{sel}=10^{-10}$ a.u. The transition energies calculated with these thresholds differed by less than 1 cm^{-1} from those reported below.
2. **g** tensor calculations were performed using unselected MRCI-S calculations on the basis of the CASSCF(3,3) reference wave functions. In these calculations, all singly-excited configurations are explicitly included (at the orbital level) relative to all reference configurations that are then spin-coupled to the desired final multiplicity. In keeping with the CASSCF/CASPT2 calculations, 13 quartet and 26 doublet roots were determined in these calculations. The SOC, represented by the multicenter SOMF operator,[58] is then diagonalized in the basis of the calculated roots and first-order perturbation theory is employed to determine **g** tensors in a way closely analogous to that described above for the CASSCF/CASPT2 method.

The desirable calculation that is employing a large number of DDCI-2 or DDCI-3 roots on top of a large active space in the **g** tensor calculations is unfortunately at present not computationally feasible.

4. Results and Discussion

4.1 TrisOH complex

The TrisOH complex (Figure 1g) consists of three copper(II) centers arranged in a triangle, each having an ethylenediamine ligand and a connection to the other two copper atoms through an OH bridge. It represents the system with the spin-frustrated ground state.[42] On each copper atom, the local pseudo-tetragonal field gives rise to a splitting of the Cu 3*d* orbitals. A σ interaction with the oxygen and nitrogen atoms results in a destabilization of the in-plane 3*d* orbital that has its lobes along the sides of the triangle. This orbital is singly occupied in each of the d^9 copper centers of TrisOH (Figure 2 shows the CASSCF wave function and Figure S1 the PM-CAS wave function). In the D_3 point group of symmetry, this configuration gives rise to a $^4A_1$ and a ^2E state. Modeled by a Heisenberg spin-Hamiltonian, $\hat{H} = -2J\sum_{i,j} S_i S_j$, the interaction between these two states gives rise to an energy splitting of 3*J*. From experiment, $J \approx -105$ cm^{-1}, indicating that the isotropic exchange interaction is antiferromagnetic ($J < 0$) with a ^2E ground state.[42] The calculated ^2E and $^4A_1$ energies are listed in Table 1. It can be seen that CASSCF already indicates the ^2E state to be the ground state, ~20 cm^{-1} below the $^4A_1$ state. The gap becomes larger upon including dynamical correlation, putting the $^4A_1$ state approximately 100 cm^{-1} above the ^2E state.

The DDCI-2 result is noticeably large: a gap of 875 cm^{-1} is predicted, which is only moderately changed by the much more expensive DDCI-3 calculations. The MRCI-S calculations produce exchange couplings that are similar to the DDCI-2 results. The following observations turn out to be valid throughout this study: (a) The intra-doublet splitting reacts more strongly to dynamical correlation than the doublet–quartet splitting; (b) the doublet–quartet splitting is similar in the DDCI-2, DDCI-3, and MRCI-S calculations; (c) the MRCI-S and DDCI-2 methods give similar results for the exchange splitting, suggesting that the essential physics is covered already at this level. This is fortunate because MRCI-S calculations can be extended to many roots without undue computational problems, whereas this is unfortunately not the case for DDCI-2; (d) the DDCI-2 calculations result in a much larger doublet–quartet splitting

than CASPT2. On the basis of the recent analysis by Malrieu and co-workers[69] this might be expected because DDCI calculations include some essential higher-order terms that are missing from second-order perturbative approaches with a minimal model space. This point was further corroborated by additional calculations employing the second-order strongly contracted *N*-electron valence-space perturbation theory (NEVPT2) as implemented in the ORCA program.[70] Generally, the NEVPT2 method produces numbers that are slightly smaller than the CASPT2 transition energies for the systems under investigation. Since NEVPT2 contains essentially the same physics as CASPT2, the numbers will not be documented in detail.

If only the two doublet and one quartet roots are considered, the SOC is small, amounting to only a few wavenumbers. Remarkably, the SOC is much larger for MS-CASPT2 (including all the roots from CASSCF, i.e., 26 doublet and 13 quartet states), pointing to an effect of using correlated PM-CAS wave functions.[71] All calculated CASPT2 values are significantly lower than the experimentally determined doublet-quartet splitting of $|3J| \approx 315\ cm^{-1}$ (Ref. 42). While the underestimation of J is expected for a method that is based on second-order perturbation theory, the variational results are expected to be better. Noticeably, the DDCI-2 values appear to be too high, which is highly unusual for this method.[72]

The experimental value for $g_{||}$ is 2.32.[42] The $g\perp$ value cannot be measured directly, but was obtained from the spin Hamiltonian of a trigonal Cu_3^{II} system. For an undistorted trigonal system, the $g\perp$ value is expected to be 0.0. However, the existence of an observable EPR intensity at an angle of 0° from the axial direction required symmetry-lowering of the geometry of the TrisOH complex. By fitting the antisymmetric exchange and distortion factor of the spin Hamiltonian to the angular dependence of the single-crystal EPR spectra, (simulated) g values of 2.32, 1.25, and 0.54 were obtained for angles of 0°, 60°, and 90° from the main axis respectively. The experimental g values 2.32 and 1.21 for angles of 0° and 60° respectively were thus nicely reproduced. The g value for larger angles cannot be verified experimentally due to broadening of the spectrum and the fact that the resonance field exceeds the range of the instrument.

The calculated g values for the lowest Kramers doublet are given in Table 1. The equatorial $g_{x,y}$ factors are close to zero for all four methods, in agreement with the expected value for an undistorted trigonal TrisOH structure. The larger anisotropy between g_x and g_y calculated with MS-CASPT2 is an artifact that derives from mixing of wave functions of different symmetry during the multistate step. Upon lifting the degeneracy of the ground state ^{2}E components, both $g\perp$ values quickly increase in magnitude.

The g_z value of 2.550 of CASSCF is significantly larger than the g_z values of CASPT2, MS-CASPT2 and MRCI-S, 2.486, 2.469 and 2.457, respectively. This is because the excitation energies of the LF states increase when dynamical correlation is included, thereby leading to smaller g values. Compared to the experimental $g_{||}$ value of 2.32, the calculated values are too high because the description of the ground state is too ionic.[18] However, there is no practical solution to this, as the charge-transfer states that would have to be included in the sum-over-states description are too high in energy and there are too many LF states below them.

The main contributions to G_{zz} arises from the ground state and a ligand-field excited ^{2}E state. They are listed in the bottom section of Table 1, showing that both contributions make up a large part of the total value. The partially-occupied natural orbitals of the contributing excited state are shown in Figure S2 for the CASSCF wave functions, and in Figure S3 for the PM-CAS wave functions. We find that both components of the excited ^{2}E state correspond to a net excitation of one electron out of the non-bonding Cu 3*d* orbital that has its lobes in between the sides of the Cu_3 triangle to the singly occupied Cu 3*d* orbital in the ground state. These correspond to the orbitals that are also involved in the LF excitation causing the local g_z value

to deviate from g_e, in case of a single copper center. These results are in agreement with the analysis carried out by Yoon and Solomon.[42]

4.2 Models of MCO intermediates

Unlike TrisOH, the four structural models for the intermediates in the reaction cycle of multicopper oxidases have no symmetry (Figure 3). All complexes are in the Cu_3^{II} redox state, resulting in two ^{2}A states and one ^{4}A state as possible candidates for the ground state. The arrangement of the ligands around each copper center gives rise to a splitting of the *d* orbitals, and the most destabilized orbital will be singly occupied in the ground state.

The Native Intermediate (NI_C and NI_S models)—For the native intermediate (NI), there are two models with different binding modes: NI_C has O^{2-} binding in the center of the three copper atoms and one OH^- as a bridging ligand, while NI_S has three OH^- ligands bridging each Cu–Cu pair. The net charge of both systems is +3. The structures of the two models are depicted in Figures 3a and 3b. The ground-state singly-occupied molecular orbitals (SOMOs) in NI_C can be approximately described within C_S symmetry, with the mirror plane perpendicular to the Cu–Cu axis of the OH^- bridged copper atoms. The singly-occupied *d* orbitals of the bridged copper atoms are similar to those of the TrisOH complex, lying in the Cu_3 plane with their lobes pointing towards the central O^{2-} moiety and the bridging OH^- ligand respectively. However, the third copper atom has its singly occupied *d* orbital perpendicular to the Cu_3 plane, with its lobes pointing towards the central oxygen atom and the axial ammonia ligands. The resulting SOMOs are visualized in Figure S4 (CASSCF) and Figure S5 (PM-CAS). In the case of NI_S, the situation is less clear, as there is no approximate symmetry. While the connectivity is the same as in TrisOH, the structure of NI_S is severely distorted from D_3 symmetry. The singly-occupied 3*d* orbitals of the two copper atoms with three ammonia ligands have the lobes in the Cu_3 plane pointing towards the OH^- ligands. The third copper atom has only two ammonia ligands arranged in a pseudo axial field. The singly occupied 3*d* orbital of this copper resembles a d_{z^2} orbital perpendicular to the Cu_3 plane. The SOMOs of NI_S are visualized in Figures S6 (CASSCF) and S7 (PM-CAS).

Experimentally, the ground state of the native intermediate is a doublet state with a low-lying excited doublet state at about 150 cm^{-1}, and a quartet excited state at about 350–900 cm^{-1} (Ref. 35). The calculated excitation energies of the lowest doublet and quartet states are given in Table 2 (NI_C) and 3 (NI_S) together with the *g* factors of the lowest Kramers doublet. Except for CASPT2 in case of NI_C, the calculated order of the states is the same as found experimentally, that is two low-lying doublet states and a higher lying quartet state. For NI_C CASPT2 predicts the quartet state at 86 cm^{-1}, in between the doublet states. With MS-CASPT2 the quartet again becomes the highest of the three states at 323 cm^{-1}, well above the excited doublet state at 129 cm^{-1}. With the latter method, the calculated splitting between the two excited states 2^2A, 1^4A is significantly larger for NI_C, 200 cm^{-1}, than for NI_S, only 50 cm^{-1}. The DDCI-2 and DDCI-3 calculations predict the position of the excited doublet state well, but predict a considerably higher energy than CASPT2 for the quartet states in both molecules. A similar result was also found for the TrisOH model complex. Overall, there are no large deviations with respect to what is expected from the experimental data. The position of the excited quartet state appears to be bracketed by the numbers from CASPT2 (tending to underestimate it) and DDCI-2/3 (tending to overestimate it).

According to the various CASPT2 variants, the calculated *g* factors differ substantially between the two models. A first observation is that the average *g* values of NI_C are smaller than those of NI_S, 2.111– 2.194 compared to 2.222–2.303. With all three methods, the *g* factors of NI_C reflect an approximate tetragonal symmetry, one value deviating much more from g_e than the other two values (with a slight deviation for MS-CASPT2). The main axis of the largest g_3

factor (2.282) is perpendicular to the C_S plane (cf. Fig. 3). Of the other two smaller *g* factors, g_2 (2.119) has its main axis perpendicular to the Cu_3 plane while the g_1 (1.951) axis goes through O^{2-} and OH^-. The *g* factors of NI_S are not rhombic and consist of three more equally spaced values. The main axis of the largest g_3 factor (2.503) lies in the Cu_3 plane, passing through its center and through the middle of the longest Cu3–O–Cu3' bridge. The main axis of g_2 (2.236) is also in-plane and perpendicular to the g_3 axis. The principal axis of the smallest g_1 (2.020) factor is perpendicular to the Cu_3 plane. For NI_C only, g_3 has an important positive contribution coming from an excited state. The contributing state corresponds to a single-electron excitation localized on the non-bridged copper atom, from the 3*d* orbital that has its lobes between the ligands to the ground-state SOMO on the same center (with lobes pointing to the ligands). For NI_S, there are two important positive contributions, both from excited states for which an electron leaves a 3*d* orbital on the copper center with pseudo-axial symmetry (two ammonia ligands). The lower of those two states contributes to the largest *g* value, the higher state to the middle *g* value. The $g < 2$ values are caused by the second doublet state. This is because SOC mixes the excited doublet state into the ground-state Kramers doublet, thereby causing the contribution from the lowest doublet to become smaller.

The MRCI-S predictions differ substantially from the CASPT2 values. Here, NI_C and NI_S have two *g* values far below 2. Interestingly, NI_C is predicted to have the third *g* value close to 2, while for NI_S a rather normal g_3 (g_z) value of 2.429 is predicted. Apparently, the MRCI-S predictions for NI_S are in best agreement with experiment where *g* values of 2.15, 1.85, and 1.65 have been reported as (g_{max}, g_{mid}, g_{min}) values.[35]

Given that the CASPT2 and MRCI-S predictions are so different, it is necessary to try to obtain some insight to what factor the *g* value predictions are particularly sensitive. The size of the $g < 2$ values is thus indirectly related to the amount of SOC between the lowest two doublet states. It is clear that to second order, excitations from doubly-occupied to singly-occupied molecular orbitals can only produce positive *g* shifts.[49] Hence, the *g* values below 2 represent higher-order contributions in the SOC that are most conveniently picked up by the QDPT procedure. This is readily seen from the third-order equation of Atkins and Jamieson where terms of the form $\langle Y_0|H^{SOC}|Y_K\rangle\langle Y_K|H^{ZE}|Y_L\rangle\langle Y_L|H^{SOC}|Y_0\rangle\{(E_0 - E_K)(E_0 - E_L)\}^{-1}$ arise in the **g** tensor expression.[73] Hence, if either the excited state K or L is equal to the second doublet and the two excited states have a nonzero Zeeman matrix element, important contributions arise to the **g** tensor that are sensitive to the splitting between the two lowest Kramers doublets. Indeed, artificially lowering the gap between the latter states causes the $g < 2$ values to drop. This also explains why there is a *g* value smaller than g_e for NI_C at the MS-CASPT2 level, but not at the CASSCF or CASPT2 level, since the amount of SOC in the latter cases is much smaller. The opposite is true for NI_S, where SOC is smaller when using the multistate procedure. The relationship between the $g < 2$ values and the amount of SOC between the two lowest doublets can be studied by lowering the energy gap between them. The results of this exercise are shown in Figure 4. The gap between the lowest doublet states was systematically reduced to 50%, 25%, 10%, and 1% of the original size for each of the methods and for both complexes. Note that the orientation of the *g* factors does not necessarily stay constant when the gap is decreased. We can see that smaller energy gaps give rise to a larger mixing of the second doublet state in the ground-state Kramers doublet (blue line). Two *g* values eventually become smaller than g_e. The evolution of the *g* factors is very similar for all methods. For the two NI models, we can make the following two distinctions: (i) while in NI_C the largest *g* value remains essentially constant, the largest *g* value of NI_S drops toward g_e near small energy gaps; (ii) the $g < 2$ values of NI_C are smaller than those of NI_S at similar energy gaps, which is demonstrated by the larger contribution of the second doublet state in NI_C with respect to NI_S. The main difference between CASSCF and CASPT2 on the one hand and MS-CASPT2 on the other hand is the larger SOC in the latter case, with smaller *g* factors for similar energy gaps as a result.

The Oxidized Resting-State Model—The oxidized resting state (Oxi) has an OH^- ligand bridging one copper pair and another OH^- ligand on the third copper atom. With all copper ions in their +II oxidation state, this results in a net charge of +4. The ground-state SOMOs of Oxi (shown in Figures S8 and S9) can be characterized using approximate C_S symmetry with the mirror plane perpendicular to the Cu–Cu axis of the OH^- bridged copper atoms. One SOMO (a) is localized on the isolated copper atom and is essentially the singly-occupied *d* orbital on that atom, perpendicular to the Cu_3 plane with its lobes pointing towards the ligands. The other two SOMOs (b and c) are bonding and antibonding combinations of the singly occupied *d* orbitals on the bridged copper atoms. The excitation energies of the lowest doublet and quartet states are presented in Table 4. One observes fairly close agreement between CASPT2 and DDCI-2/3 or MRCI-S for the position of the first doublet excited state. However, the quartet is again predicted considerably higher in energy by the variational methods.

The first excited doublet state and the lowest quartet state are close in energy for the CASPT2-based calculations methods, with the CASPT2 and MS-CASPT2 energies similar in size, about 3 times larger than the CASSCF energies. The pattern obtained from the calculated energy splittings by the perturbational methods indicates the strong AF coupling of the two T3-Cu centers (whereas T2 center does not couple to T3), in agreement with the experimental findings.[74] Quantitatively, the doublet– quartet energy gap, $\Delta E_{D\text{-}Q} > 400\ cm^{-1}$ ($J < -200\ cm^{-1}$),[74] is only slightly underestimated by the CASPT2 methods and overestimated by the DDCI-*n* and MRCI-S methods.

The main axis of the largest g_3 factor is oriented along the Cu–Cu bond of the bridged copper atoms, while the smaller (and similar) g_1 and g_2 factors have their axes oriented in-plane ($\perp g_3$) and perpendicular to the Cu_3 plane, respectively. The direction of g_3 corresponds to the local magnetic axis of an approximately tetragonal copper center. The main excited state contribution here comes from an excitation from the *d* orbital with its lobes between the ligands to the GS SOMO as shown in Figures S8 and S9. This is also the only important excited-state contribution.

The experimental values of $g_x = 2.04$, $g_y = 2.05$, $g_z = 2.24$ have been reported.[75] Assuming a systematic overestimation of $g_\parallel$ values, as was observed for the TrisOH and NI systems, we consider the agreement between MS-CASPT2 values and the experiment as reasonable and qualitative. The MRCI-S method, on the other hand, severely underestimates the $g\perp$ values, which is surprising given that the intra-doublet splitting is similar to the CASPT2 values. We may only assume this observation can be attributed to the third (and higher) order effects. A careful analysis of these contributions is involved and has not been attempted in the present paper.

The Peroxy Adduct (PA)—The peroxy adduct (PA_C) has a peroxide moiety (O_2^{2-}) binding in the center of the trinuclear Cu_3 cluster and an OH^- ligand on one of the copper atoms. One of the peroxide oxygen atoms bridges two copper atoms, while the other oxygen atom is bound to the third copper atom. The resulting bonding arrangement is asymmetric, making it difficult to characterize the SOMOs of the ground state (Figures S10 and S11). As for the singly occupied *d* orbitals, the one associated with the copper atom with two oxygen ligands is clearly perpendicular to the Cu_3 plane, with lobes pointing towards the tetragonally arranged ligands. The singly-occupied *d* orbitals of the other two copper atoms have a less clear orientation. The arrangement can be seen as pseudo-tetrahedral, with the lobes of the singly-occupied *d* orbitals pointing along the bonds to the surrounding ligands, forming a weakly bonding and antibonding combination.

The excitation energies of the lowest doublet and quartet states are presented in Table 5. The comparison between CASPT2 and the variational approaches follows the established trends.

However, here the large increase of the excited doublet state in going from DDCI-2 to DDCI-3 is certainly noteworthy. Also notable is the extremely large change in energy of the first excited quartet state when going from the perturbational to the variational approaches. Here, the discrepancy between CASPT2 and the DDCI methods approaches a full order of magnitude.

The highest doublet and quartet states are close in energy, 25 cm^{-1} at the CASSCF level, and 90 cm^{-1} at the CASPT2 level. When the multistate procedure is used, the quartet state at 165 cm^{-1} drops below the second doublet state at 220 cm^{-1}. The largest g_3 factor is oriented perpendicular to the bridged copper bond. The g_1 axis is also oriented in-plane, perpendicular to the g_3 axis, while the g_2 axis is oriented perpendicular to the Cu_3 plane. There are three major excited-state contributions, all with respect to g_3, from excited states corresponding to a single-electron excitation on each of the copper centers. These involve two *d* orbitals with their lobes pointing towards and in between the ligands, respectively. The analysis of these excited states is in this case not straightforward, as the single-electron excitations are not clearly located on a specific center. Based on CASSCF wave functions, the largest positive contribution comes from the 19^2A state, while the 11^2A and 13^2A states give similar negative and positive contributions (Figure S10). However, with PMCAS wave functions, 11^2A and 12^2A give a positive contribution and 14^2A a negative contribution.

Again, the MRCI-S values are completely different from any of the CASPT2 predictions. Rather, an EPR spectrum resembling that of the NI_C model is predicted in which two *g* values are significantly below 2 and the third one stays close to the free electron *g* value with a positive deviation from it.

The closest experimental system to compare our data with is an adduct of the resting oxidized state with azide (denoted NI_{Az}).[76] The experimental data indicate a presence of low-lying doublet state (~30 cm^{-1}) and $g_{\perp}^{eff}=1.86$ and $g_{\parallel}^{eff}=2.33$ values. Assuming the similarity of the two systems (the experimental NI_{Az} and the calculated PA_C) we can see that MS-CASPT2 overestimates $g_{\perp}^{eff}$ value by 0.15 resulting in a wrong sign of the Δg value, whereas it predicts $g_{\parallel}^{eff}$ with a reasonable accuracy. The MRCI-S method is in qualitative accordance with experiment. It does correctly predict a negative *g* shift for $g_{\perp}^{eff}$, but somewhat surprisingly it significantly underestimates the $g_{\parallel}^{eff}$ value. However, both methods predict a higher intra-doublet splitting for PA_C (with respect to the NI_{Az}), although it is difficult to assess its exact value for the PA_C intermediate.

4.3. Methodological Aspects

As has been already mentioned, the presented calculations probably represent the current state-of-the-art of quantum chemical methodology in the calculations of EPR parameters for three-spin coupled systems. The calculations presented were preceded by extensive efforts, mostly on the model TrisOH system that have demonstrated that the adopted computational protocols are most likely the only strategies currently available in modern quantum chemistry program packages yielding qualitatively and perhaps even semiquantitatively correct results. These efforts included a careful testing of basis-set dependence, size of the active space, CASSCF state-averaging, size of MRCI reference space and its truncation (e.g., *a posteriori* selection of configurations, including the DDCI-2 and DDCI-3 methods), and alternative approaches to calculate **g** tensors (e.g., linear-response theory) have also been tested, but they were not successful since the g-tensors are dominated by higher-order SOC effects in the case of copper trimers.

Concerning the comparison of CASPT2 and MRCI-S approaches, it can be seen in Tables 2–5 that in many cases, the performance of the two methods is fairly similar with respect to the

calculated doublet splittings. However, both approaches produce considerably smaller splittings than DDCI-2 and DDCI-3, which would seem to indicate that some important higher-order effects are missed in both approaches. This is even more evident for the doublet–quartet splittings that are considerably larger in all variational methods compared to the CASPT2 calculations. The two comparisons with experimental data concern the native intermediate, which has a $1^2A–2^2A$ splitting[35] of ~150 cm^{-1}, and the TrisOH system, which has a zero-field splitting for the ^2E state of ~65 cm^{-1}. Both are reproduced reasonably well by CASPT2. MRCI-S provides a good value for the intra-doublet splitting, but substantially underestimates the zero-field splitting in TrisOH. Unfortunately, the more rigorous DDCI-2 and DDCI-3 methods are computationally too expensive to calculate enough states for quasi-degenerate perturbation theory to deliver reasonably converged magnetic properties. On the other hand, the MRCI-S method has the advantage that it leads to a consistent set of mutually orthogonal and variationally optimized excited states that form a straightforward expansion basis for the QDPT procedure.

For the **g** tensors, the results from CASPT2 and MRCI-S differ substantially. Experimentally, *g* values of 2.15, 1.85, and 1.65 have been reported for the native intermediate as a spin-frustrated system with all three copper ions coupled by the O^{2-} bridge to yield the ground state doublet. The only calculation that leads to even qualitative agreement appears to be MRCI-S. However, MRCI-S fails to reproduce the T2-Cu EPR signal ($g_x = 2.04$, $g_y = 2.05$, $g_z = 2.24$) in the resting oxidized form, whereas the MS-CASPT2 reproduced these value at least qualitatively. A less straightforward comparison between experimentally studied azide adduct of the native intermediate and the theoretically calculated peroxy adduct (PA_C) showed similar trends as observed in Oxi, an overestimation of the *g* values by MS-CASPT2 and their underestimation by MRCI-S.

One problem with all methods tested here is that the results suffer from the inherently poor covalency of the parent CASSCF wave function that cannot be repaired by the moderate correlation treatment brought in by the singles (MRCI-S) or are not changed at all (CASPT2). This must introduce important errors in the SOC matrix elements that will ultimately affect the accuracy of the ***g***-tensor calculations. The results obtained for the most well characterized complex of this study, TrisOH, are typical in this respect.

It is evident that for nearly orbitally degenerate systems, the *g* values are extremely sensitive to even small changes in the splittings of the lowest doublets and quartets. Such small variations may arise from subtle changes in geometry and are possibly influenced by environmental and basis-set effects or vibronic coupling. Hence, the accurate description of these small effects is inherently difficult for all theoretical methods, and much more extensive comparisons between theory and experiment for well-defined model systems are necessary to understand the scope and limitations of the current theoretical methods more comprehensively. However, in principle, theoretical calculations can serve as a tool assisting us in distinguishing between several structural alternatives or at least suggesting that the studied models are in accordance with the experimentally measured EPR spectra.

5. Conclusions

In this work, we present the results of multireference *ab initio* calculations of zero-field splittings and **g** tensors of model systems representing the intermediates in the MCO reaction cycle. It was shown that only those approaches represented by the CASSCF/CASPT2, MRCI-S and DDCI-2/3 methods can yield (at least) qualitatively correct results. It is, at this point, extremely difficult to treat all contributions to the system **g** tensor (an extreme case is represented by the TrisOH model complex) on an equal footing and obtain quantitative agreement with experiment, since calculations such as MRCI-SD (with 27-in-15 active space)

or size-consistent variants of it that might represent the next step in the "ladder of accuracy" are, so far, prohibitively expensive. In addition, the size-consistency problems of the MRCI method must be addressed before good result can be expected, even if the calculations would be feasible. However, the presented study represents an important step towards rigorous and accurate calculations of spectroscopic properties of bioinorganic systems with complicated electronic structures, involving spin interactions of several open-shell centers. Moreover, we provided a theoretical interpretation of the peculiarities observed in the EPR spectra of MCO intermediates in terms of the excited electronic states contributing to the **g** tensors and quantitatively evaluated the antisymmetric exchange mechanism formulated in previous work.[42–45]

Supplementary Material

Refer to Web version on PubMed Central for supplementary material.

Acknowledgments

This work has been supported by grants LC512 and Z40550506 (MSMT CR) and by grants from the Flemish Science Foundation (FWO) and the Concerted Research Action of the Flemish Government (GOA). SV thanks the University of Leuven (BOF) for financial support. FN gratefully acknowledges financial support by the SFB 813 (Chemistry at spin centers) and by the University of Bonn. EIS acknowledges the NIH DK31450 for financial support.

REFERENCES

1. Telser, J., editor. See e.g. Paramagnetic Resonance of Metallobiomolecules (ACS Symposium Series). American Chemical Society; 2003.
2. Moores WH, McWeeny R. Proc. R. Soc. A-Math. Phys. Eng. Sci 1973;332:365–384.
3. Lushington GH, Grein F. J. Chem. Phys 1997;106:3292–3300.
4. Vahtras O, Minaev B, Ågren H. Chem. Phys. Lett 1997;281:186–192.
5. Neese, F.; Solomon, EI. Magnetoscience – From Molecules to Materials. Drillon, M.; Miller, JS., editors. Vol. Vol. IV. New York: Wiley; 2003. p. 345
6. Neese F. Curr. Opin. Chem. Biol 2003;7:125–135. [PubMed: 12547437]
7. Neese F. Magn. Reson. Chem 2004;42:S187–S198. [PubMed: 15366053]
8. Neese, F. Specialist Periodical Reports on EPR Spectroscopy. Gilbert, B., editor. Vol. Vol. 20. Royal Society Press; 2006.
9. Neese, F. Current Topics in Chemistry. Reiher, M., editor. Springer, Heidelberg; 2006.
10. Sinnecker, S.; Neese, F. Biological Magnetic Resonance. Hanson, G.; Berliner, L., editors. 2009.
11. Neese, FCoord. Chem. Rev 2009;253:526–563.
12. Malkina OL, Vaara J, Schimmelpfennig B, Munzarova M, Malkin V, Kaupp M. J. Am. Chem. Soc 2000;122:9206–9218.
13. Vahtras O, Engström M, Schimmelpfennig B. Chem. Phys. Lett 2002;351:424–430.
14. Neese F. Chem. Phys. Lett 2003;380:721–728.
15. Neese F. J. Chem. Phys 2001;115:11080–11096.
16. Neese F. J. Chem. Phys 2003;117:3939–3948.
17. Vancoillie S, Malmqvist P-Å, Pierloot K. ChemPhysChem 2007;8:1803–1815. [PubMed: 17647251]
18. Vancoillie S, Pierloot K. J. Phys. Chem. A 2008;112:4011–4019. [PubMed: 18386853]
19. Rinkevicius Z, de Almeida KJ, Vahtras O. J. Chem. Phys 2008;129:064109. [PubMed: 18715053]
20. Neese, FInt. J. Quant. Chem 2001;83:104–114.
21. Neese F. J. Phys. Chem. A 2001;105:4290–4299.
22. Neese F, Goldfarb D. J. Am. Chem. Soc 2006;128:2017–2029. [PubMed: 16464103]
23. Kababya S, Nelson J, Calle C, Baute D, Arieli D, Zimmermann H, Neese F, Weckhuysen B, Goldfarb D. J. Am. Chem. Soc 2004;126:11733–11745. [PubMed: 15366921]

24. Mezei G, Raptis RG, Telser J. Inorg. Chem 2006;45:8841–8843. [PubMed: 17054337]
25. Vancoillie S, Rulíšek L, Neese F, Pierloot K. J. Phys. Chem. A 2009;113:6149–6157. [PubMed: 19413285]
26. Ovcharenko VI, Fokin SV, Romanenko GV, Shvedenkov YG, Ikorskii VN, Tretuakov EV, Vasilevskii SF. J. Struct. Chem 2002;43:153–167.
27. Fedin MV, Veber SL, Gromov IA, Ovcharenko VI, Sagdeev RZ, Schweiger A, Bagryanskaya EG. J. Phys. Chem. A 2006;110:2315–2317. [PubMed: 16480287]
28. Veber SL, Fedin MV, Potapov AI, Maryunina KY, Romanenko GV, Sagdeev RZ, Ovcharenko VI, Goldfarb D, Bagryanskaya EG. J. Am. Chem. Soc 2008;130:2444–2445. [PubMed: 18232693]
29. Solomon EI, Sundaram UM, Machonkin TE. Chem. Rev 1996;96:2563–2605. [PubMed: 11848837]
30. Messerschmidt, A. Multicopper oxidases. Messerschmidt, A., editor. Singapore; River Edge, NJ: World Scientific; 1997. p. 23-80.
31. Xu F. Biochemistry 1996;35:7608–7614. [PubMed: 8652543]
32. Davies, GJ.; Ducros, V. Handbook of Metalloproteins. Messerschmidt, A.; Huber, R.; Wieghardt, K.; Poulos, T., editors. New York: Wiley; 2001. p. 1359-1368.
33. Shin W, Sundaram UM, Cole JL, Zhang HH, Hedman B, Hodgson KO, Solomon EI. J. Am. Chem. Soc 1996;118:3202–3215.
34. Palmer AE, Lee S-K, Solomon EI. J. Am. Chem. Soc 2001;123:6591–6599. [PubMed: 11439045]
35. Lee S-K, George SD, Antholine WE, Hedman B, Hodgson KO, Solomon EI. J. Am. Chem. Soc 2002;124:6180–6193. [PubMed: 12022853]
36. Piontek K, Antorini M, Choinowski T. J. Biol. Chem 2002;277:37663–37669. [PubMed: 12163489]
37. Roberts SA, Wildner GF, Grass G, Weichsel A, Ambrus A, Rensing C, Montfort WR. J. Biol. Chem 2003;278:31958–31963. [PubMed: 12794077]
38. Rulíšek L, Solomon EI, Ryde U. Inorg. Chem 2005;44:5612–5628. [PubMed: 16060610]
39. Chalupský J, Neese F, Solomon EI, Ryde U, Rulíšek L. Inorg. Chem 2006;45:11051–11059. [PubMed: 17173465]
40. Ryde U, Hsiao Y-W, Rulíšek L, Solomon EI. J. Am. Chem. Soc 2007;129:726–727. [PubMed: 17243785]
41. Sundaram UM, Zhang HH, Hedman B, Hodgson KO, Solomon EI. J. Am. Chem. Soc 1997;119:12525–12540.
42. Yoon J, Mirica LM, Stack TDP, Solomon EI. J. Am. Chem. Soc 2004;126:12586–12595. [PubMed: 15453791]
43. Mirica LM, Stack TDP. Inorg. Chem 2005;44:2131–2133. [PubMed: 15792444]
44. Yoon J, Solomon EI. Inorg. Chem 2005;44:8076–8086. [PubMed: 16241158]
45. Yoon J, Mirica LM, Stack TDP, Solomon EI. J. Am. Chem. Soc 2005;127:13680–13693. [PubMed: 16190734]
46. Neese F. Mol. Phys 2007;105:2507–2514.
47. Malrieu JP, Heully JL, Zaitsevskii A. Theor. Chim. Acta 1995;90:167–187.
48. Ganyushin D, Neese F. J. Chem. Phys 2006;125:024103.
49. Neese F, Solomon EI. Inorg. Chem 1998;37:6568–6582. [PubMed: 11670788]
50. Gerloch M, McMeeking RF. J. Chem. Soc., Dalton Trans 1975:2443–2451.
51. Bolvin H. ChemPhysChem 2006;7:1575. [PubMed: 16810728]
52. Tatchen J, Kleinschmidt M, Marian CM. J. Chem. Phys 2009;130:154106. [PubMed: 19388735]
53. Pierloot, K. Computational Organometallic Chemistry. Cundari, TR., editor. Marcel Dekker; 2000. p. 123-158.
54. (a) Miralles J, Castell O, Caballol R, Malrieu JP. Chem. Phys 1993;172:33–43. (b) Garcia VM, Castell O, Caballol R, Malrieu JP. Chem. Phys. Lett 1995;238:222–229. (c) Calzado CJ, Cabrero J, Malrieu JP, Caballol R. J. Chem. Phys 2002;116:3985–4000.
55. Ganyushin D, Hansen A, Liakos DG, Kollmar C, Kossmann S, Petrenko T, Reimann C, Riplinger C, Sivalingam K, Valeev E, Wezisla B, Wennmohs F. ORCA is an ab initio, density functional and semi-empirical program package written by Neese, F. with contributions from Becker, U.
56. Hess BA, Marian CM, Wahlgren U, Gropen O. Chem. Phys. Lett 1996;251:365–371.

57. Christiansen O, Gauss J, Schimmelpfennig B. PhysChemChemPhys 2000;2:965–971.
58. Neese F. J. Chem. Phys 2005;122:034107.
59. Malmqvist P-Å, Rendell A, Roos BO. J. Phys. Chem 1990;94:5477–5482.
60. Andersson K, Malmqvist P-Å, Roos BO, Sadlej AJ, Wolinski K. J. Phys. Chem 1990;94:5483–5488.
61. Andersson K, Malmqvist P-Å, Roos BO. J. Chem. Phys 1992;96:1218–1226.
62. Karlström G, Lindh R, Malmqvist P-Å, Roos BO, Ryde U, Veryazov V, Widmark P-O, Cossi M, Schimmelpfennig B, Neogrady P, Seijo L. Comput. Mater.Sci 2003;28:222–239.
63. Pierloot K, Dumez B, Widmark P-O, Roos BO. Theor. Chim. Acta 1995;90:87–114.
64. Finley J, Malmqvist P-Å, Roos BO, Serrano-Andrés L. Chem. Phys. Lett 1998;288:299–306.
65. Hess BA, Marian CM, Wahlgren U, Gropen O. Chem. Phys. Lett 1996;251:365–371.
66. Christiansen O, Gauss J, Schimmelpfennig B. PhysChemChemPhys 2000;2:965–971.
67. Weigend F, Ahlrichs R. Phys. Chem. Chem. Phys 2005;7:3297–3305. [PubMed: 16240044]
68. Neese F. J. Chem. Phys 2003;119:9428–9443.
69. Calzado CJ, Angeli C, Taratiel D, Caballol R, Malrieu JP. J. Chem. Phys 2009;131:044327. [PubMed: 19655887]
70. Sivalingam K, de Angeli C, Neese F. ms in preparation.
71. We tend to believe that CASSCF suffers from the poor covalency leading to too little metal-ligand overlap and hence too small multicenter SOC. In CASPT2 the CASSCF wave function is used to calculate all matrix elements and hence the shortcomings are not remedied. In MS-CASPT2, states are allowed to mix and hence one obtains a correlated wave function that does remedies part of the shortcomings of CASSCF/CASPT2.
72. Illas F, Moreira IDR, de Graaf C, Barone VTheor. Chem. Acc 2000;104:265–272.
73. Atkins PW, Jamieson AM. Mol. Phys 1967;14:425–431.
74. Cole JL, Clark PA, Solomon EI. J. Am. Chem. Soc 1990;112:9534–9548.
75. Quintanar L, Yoon J, Aznar CP, Palmer AE, Andersson KK, Britt RD, Solomon EI. J. Am. Chem. Soc 2005;127:13832–13845. [PubMed: 16201804]
76. Yoon J, Liboiron BD, Sarangi R, Hodgson KO, Hedman B, Solomon EI. Proc. Natl. Acad. Sci. U. S. A 2007;104:13609–13614. [PubMed: 17702865]

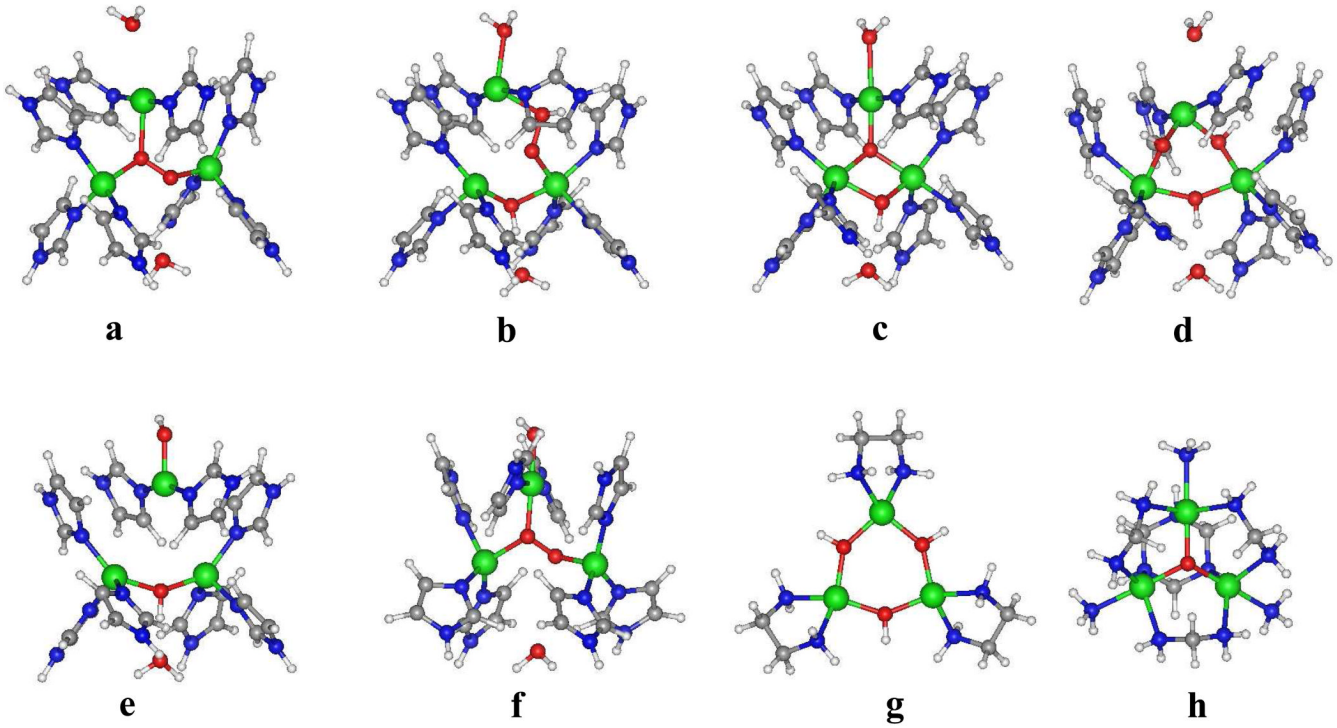

Figure 1.

Structural models of the various MCO states and inorganic models of the NI as suggested by spectroscopic measurements and QM/MM calculations:[34,35, 38,39,40] (a) PI_C, (b) PI_S, (c) NI_C, (d) NI_S, (e) oxidized resting state, (f) PA_C, (g) TrisOH and (h) μ_3O (color scheme: green -copper ions, red – oxygens, blue- nitrogens grey – carbons, white - hydrogens).

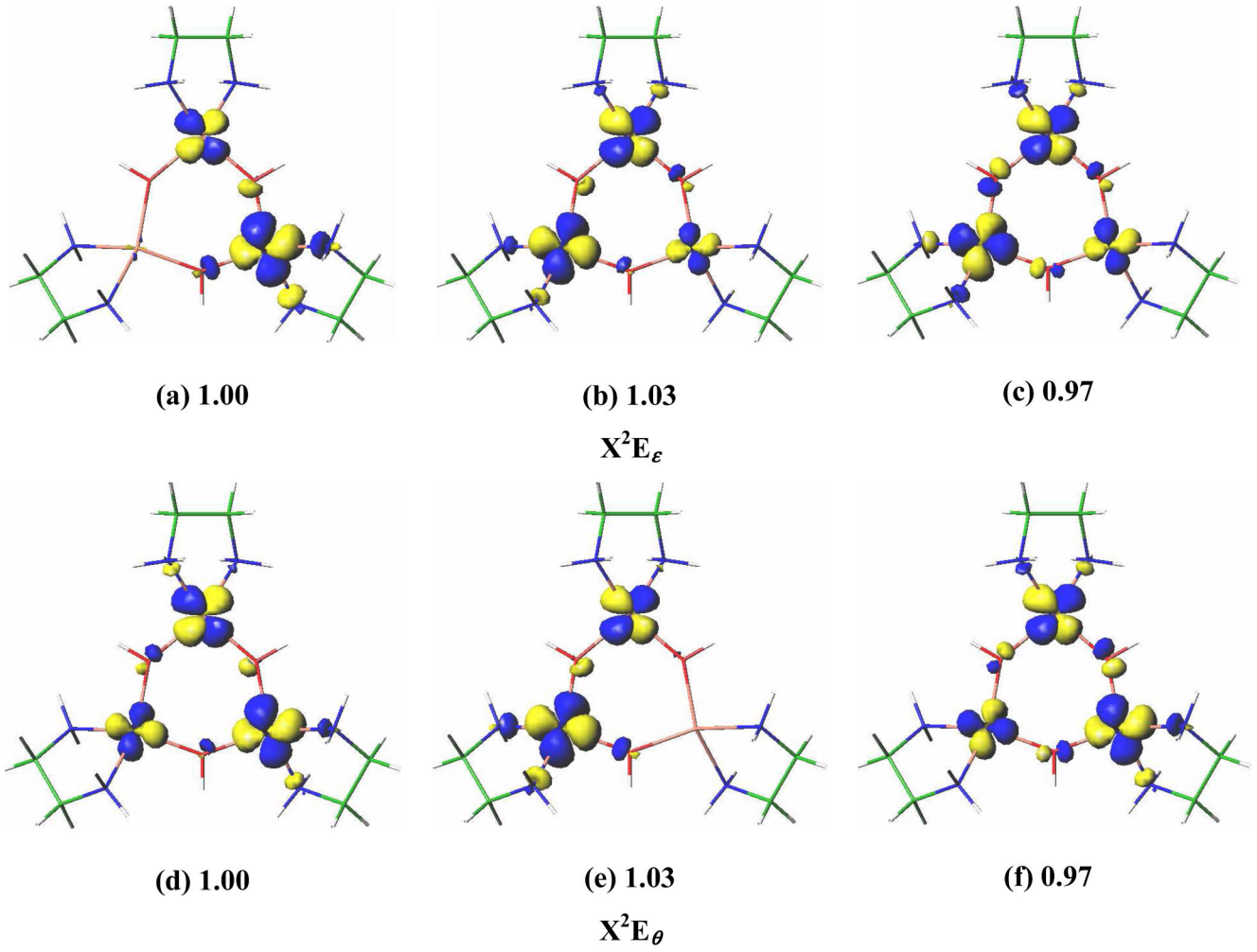

Figure 2.
The ground-state X^2E SOMOs of the TrisOH complex, calculated at the CASSCF level.

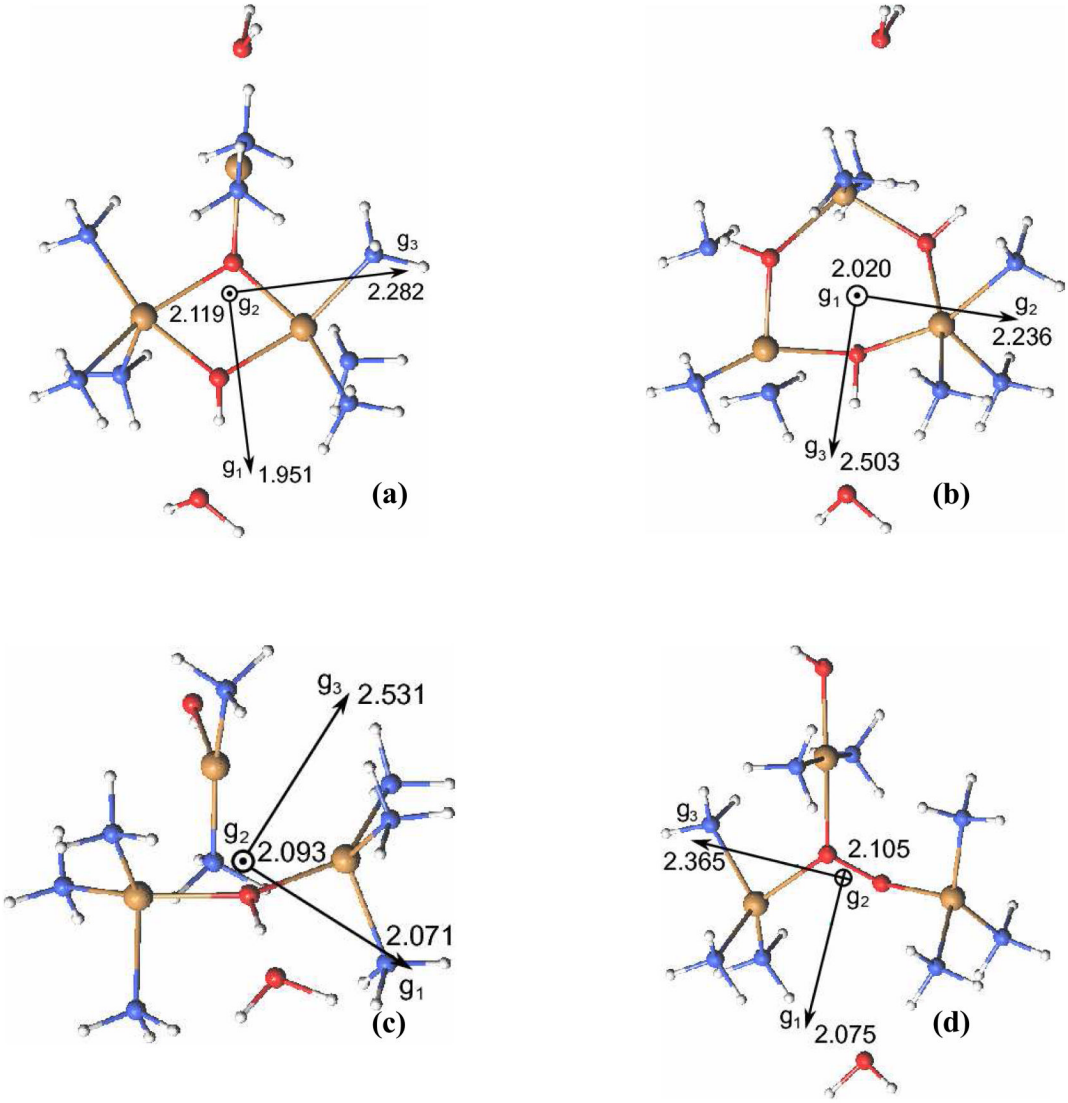

Figure 3.

Models of MCO intermediates. (a) NI_C, (b) NI_S, (c) oxidized resting state and (d) PA_C, The key geometric parameters are identical to those of the large models in Figure 1 but in the present models imidazole ligands are replaced by ammonia. This approximation was previously shown to be reasonable (Ref 39). The main axes of the calculated **g** tensors are also included.

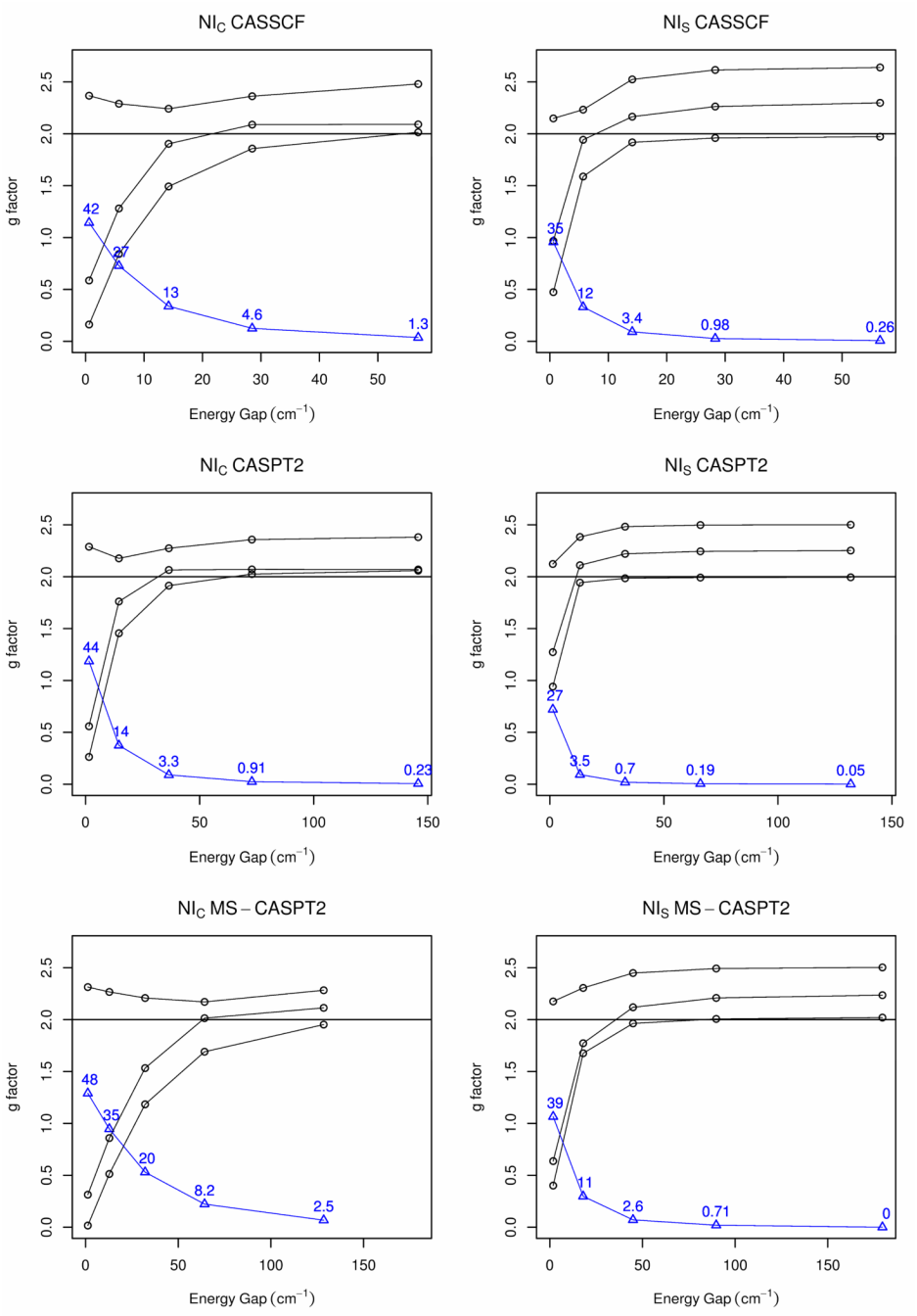

Figure 4.

Dependence of the *g* values of NI$_C$ and NI$_S$ on the size of the energy gap between the lowest two doublet states. Black circles show the calculated *g* values, whereas blue triangles with labels indicate the percentage of excited doublet state entering the ground-state Kramers doublet.

Table 1

Excitation energies of the lowest doublet and quartet states (cm^{-1}), and principal g values of the lowest Kramers doublet with indication of the main contributing states of TrisOH.

	CASSCF		CASPT2		MS-CASPT2		DDCI-2[d]	DDCI-3[d]	MRCI-S	
X^2E	0[a]	0[b]	0[a]	0[b]	0[a]	0[b]	0	0	0[a]	0[b]
		17		18		88				24
1^4A_1	23	29	105	108	112	150	875	718	869	856
		31		110		152				
g_x		0.086		0.079		0.098			0.055	
g_y		0.086		0.079		0.053			0.055	
g_z		2.550		2.486		2.469			2.457	
States	ΔE	ΔG_{zz}	ΔE	ΔG_{zz}	ΔE	ΔG_{zz}				
X^2E	0	3.765	0	3.818	0	3.826				
2^2E[c]	8462	2.487	9654	2.182	9658	2.039				
All		6.502		6.178		6.097				

[a] One-component relativistic (without SOC) states obtained from CASSCF(27,15)/CASPT2/MS-CASPT2, averaging over all 26 doublet and 13 quartet states and including all roots in the multi-state procedure. The ORCA CASSCF(3,3) calculations with the def2-SV(P) basis set yield 23 cm^{-1} for the position 1^4A_1.

[b] Two-component relativistic (with SOC) states

[c] For MS-CASPT2, this is in fact the second excited ^2E state. Due to symmetry-breaking, a small contribution from another state is also included.

[d] Based on a SA-CASSCF(3,3) reference, averaged over the lowest two doublet and one quartet states. Truncation thresholds were $T_{sel}=10^{-8}$ a.u., $T_{pre}=10^{-5}$ a.u.

Table 2

Excitation energies of the lowest doublet and quartet states (cm^{-1}) and principal g values of the lowest Kramers doublet of NI_C.

	CASSCF		CASPT2		MS-CASPT2		DDCI-2[c]	DDCI-3[c]	MRCI-S
X^2A	0[a]	0[b]	0[a]	0[b]	0[a]	0[b]	0	0	0
2^2A	57	58	146	145	130	133	106	174	99
1^4A_1	91	91	86	86	323	323	1451	1619	1398
		92		89		327			
g_1		2.014		2.058		1.951			1.581
g_2		2.090		2.069		2.119			1.824
g_3		2.479		2.381		2.282			2.010

[a] One-component relativistic (without SOC) states obtained from CASSCF(27,15)/CASPT2/MS-CASPT2 averaging over all 26 doublet and 13 quartet states and including all roots in the multi-state procedure. The ORCA SA-CASSCF(3,3) calculations with the def2-SV(P) basis set yield 46 cm^{-1} for 2^2A and 89 cm^{-1} for 1^4A.

[b] Two-component relativistic (with SOC) states

[c] See footnote *d* of Table 1

Table 3

Excitation energies of the lowest doublet and quartet states (cm^{-1}) and principal g values of the lowest Kramers doublet of NI_S.

	CASSCF		CASPT2		MS-CASPT2		DDCI-2[c]	DDCI-3[c]	MRCI-S
X^2A	0[a]	0[b]	0	0	0	0	0	0	0
2^2A	57	56	132	131	180	178	152	336	146
1^4A_1	79	78	204	202	229	228	1096	1101	1082
		79		203		229			
g_1		1.972		1.994		2.020			1.674
g_2		2.298		2.252		2.236			1.910
g_3		2.639		2.501		2.503			2.429

[a] One-component relativistic (without SOC) states obtained from CASSCF(27,15)/CASPT2/MS-CASPT2 averaging over all 26 doublet and 13 quartet states and including all roots in the multi-state procedure. The ORCA SA-CASSCF(3,3) calculations with the def2-SV(P) basis set yield 55 cm^{-1} for 2^2A and 78 cm^{-1} for 1^4A.

[b] Two-component relativistic (with SOC) states

[c] See footnote *d* of Table 1

Table 4

Excitation energies of the lowest doublet and quartet states (cm^{-1}) and principal *g* values of the lowest Kramers doublet of oxidized resting state model (Oxi).

	CASSCF		CASPT2		MS-CASPT2		DDCI-2[c]	DDCI-3[c]	MRCI-S
X^2A	0^a	0^b	0^a	0^b	0^a	0^b	0	0	0
2^2A	110	108	307	301	322	315	308	565	297
1^4A_1	111	109	332	327	339	335	908	929	896
		109		327		335			
g_1		2.092		2.080		2.071			1.552
g_2		2.074		2.075		2.093			1.872
g_3		2.716		2.527		2.531			2.116

[a] One-component relativistic (without SOC) states obtained from CASSCF(27,15)/CASPT2/MS-CASPT2 averaging over all 26 doublet and 13 quartet states and including all roots in the multi-state procedure. The ORCA SA-CASSCF(3,3) calculations with the def2-SV(P) basis set yield 112 cm^{-1} for 2^2A and 115 cm^{-1} for 1^4A.

[b] Two-component relativistic (with SOC) states

[c] See footnote *d* of Table 1

Table 5

Excitation energies of the lowest doublet and quartet states (cm^{-1}) and principal g values of the lowest Kramers doublet of peroxy adduct model (PA_C).

	CASSCF[a]		CASPT2		MS-CASPT2		DDCI-2[c]	DDCI-3[c]	MRCI-S
X^2A	0^a	0^b	0	0	0	0	0	0	0
2^2A	23	22	85	82	221	213	81	366	77
1^4A_1	27	26	95	92	165	159	1067	1187	1057
		27		93		161			
g_1		2.038		2.022		2.076			1.685
g_2		2.112		2.101		2.105			1.853
g_3		2.383		2.315		2.365			2.080

[a] One-component relativistic (without SOC) states obtained from CASSCF(27,15)/CASPT2/MS-CASPT2 averaging over all 26 doublet and 13 quartet states and including all roots in the multi-state procedure. The ORCA SA-CASSCF(3,3) calculations with the def2-SV(P) basis set yield 23 cm^{-1} for 2^2A and 26 cm^{-1} for 1^4A.

[b] Two-component relativistic (with SOC) states

[c] See footnote *d* of Table 1